

Supporting Information

Methanol Tolerance of Atomically Dispersed Single Metal Site Catalysts: Mechanistic Understanding and High-performance in Direct Methanol Fuel Cells

Qirong Shi^{a,1}, Yanghua He^{a,1}, Xiaowan Bai^{b,1}, Maoyu Wang^c, David A. Cullen^d,
Macros Lucero^c, Xunhua Zhao^b, Karren L. More^d, Hua Zhou^c, Zhenxing Feng^{c,*},
Yuanyue Liu^{b,*} and Gang Wu^{a,*}

^aDepartment of Chemical and Biological Engineering, University at Buffalo, The State
University of New York, Buffalo, NY 14260, USA

^bTexas Materials Institute and Department of Mechanical Engineering, The University of Texas
at Austin, Austin, Texas 78712, USA

^cSchool of Chemical Biological, and Environmental Engineering Oregon State University,
Corvallis, OR 97331, USA

^dCenter for Nanophase Materials Sciences, Oak Ridge National Laboratory, Oak Ridge National
Laboratory, Oak Ridge, TN 37831, USA

^eX-ray Science Division, Argonne National Laboratory, Lemont, IL, 60439, USA

† These two authors contributed equally.

* Corresponding authors: zhenxing.feng@oregonstate.edu (Z. Feng);
yuanyue.liu@austin.utexas.edu (Y Liu); gangwu@buffalo.edu (G. Wu)

1. these two authors contributed equally.

Experimental details

Figure S1 to S19

Table S1 to S4

References

Experimental Section

Chemical and Materials

All chemical reagents including zinc nitrate hexahydrate (99%) (Alfa Aesar), cobalt(II) nitrate hexahydrate (99+%) (ACROS Organics), iron (III) chloride (Sigma Andrich), 2-methylimidazole (99%) (ACROS Organics Pluronic(R) F-127 (Sigma Andrich), methanol (99.8+%) (Fisher Chemical), 2-isopropanol (Fisher Chemical) , were used directly without further purification. The commercial 20% Pt/C catalyst was purchased from (Cabot Corp.). Commercial PtRu/C (48 wt% Pt and 24wt% Ru) was purchased from Johnson Matthey. Nafion was acquired from Sigma Aldrich.

Synthesis of Fe-doped ZIF-8-derived Fe-N-C catalysts

The synthesis of 50 nm Fe-doped ZIF-8 derived Fe-N-C catalysts was similar to the method reported previously by our group. Typically, solution A was prepared by dissolving 3.39 g $\text{Zn}(\text{NO}_3)_2 \cdot 6\text{H}_2\text{O}$ and 0.10 g $\text{Fe}(\text{NO}_3)_3 \cdot 9\text{H}_2\text{O}$ into 300 mL methanol. Solution B was prepared by dissolving 3.94 g 2-methylimidazole into another 300 mL methanol solution. Then, Solution B was added into solution A and heated at 60 °C for 24 h, followed by collecting the precipitant through washing with ethanol and dried at 60 °C in a vacuum oven. Finally, Fe-N-C catalysts were obtained after the thermal activation at 1100 °C under N_2 flow for one h in a tube furnace. No additional acidic leaching and the second heating treatment were required.

Synthesis of Fe/Co-N-C catalysts and Fe-N-C catalysts

The synthesis of Fe/Co-N-C catalysts is involved with chemical doping and adsorption steps. At first, Co-doped ZIF-8 nanocrystals were first. Typically, for Co-N-C with Zn/Co precursor feeding ratio of 11/2, solution A was prepared by dissolving 1 g Pluronic F127, 3.267 g $\text{Zn}(\text{NO}_3)_2 \cdot 6\text{H}_2\text{O}$ and 0.582 g $\text{Co}(\text{NO}_3)_2 \cdot 6\text{H}_2\text{O}$ into 100 mL methanol. Solution B was prepared by dissolving 3.2 g 2-methylimidazole into another 100 mL methanol solution. Then, Solution B was added into solution A and heated at 60 °C for one h with stirring under oil bath and refluxing condition, followed by collecting the precipitant through washing with ethanol and dried at 60 °C in a vacuum oven. Finally, Co-N-C catalysts were obtained after the thermal activation at 900 °C under N_2 flow for 1 h in a tube furnace. Co-N-C with other Zn/Co precursor ratios were obtained by just changing Zn and Co precursors amount in accordance with their ratios. In a second adsorption step, 50 mg

Co-N-C catalysts were dissolved in a vial containing 5 mL 2-isopropanol, followed by adding x mg FeCl₃ (x= 2.5, 3.0, 3.5, 4.0) and ultrasonic for 2 hrs. After 2 hrs, the mixture was stirred for another 2 hrs at room temperature. Then, the catalysts were collected by centrifugation and dried at 60 °C in a vacuum oven. Finally, the Fe/Co-N-C catalysts were obtained by thermal activation at 1100 °C under N₂ flow for one h in a tube furnace.

Fe-N-C catalysts obtained by adsorption methods were obtained via a similar method except in the first chemical-doping step without adding Co precursors. In other words, the Zn/Co precursor feeding ratio is 13/0.

Physical characterization

The morphology of M-N-C catalysts was characterized using scanning electron microscopy (SEM) on a Hitachi SU 70 microscope at a working voltage of 5 kV. The N₂ isothermal adsorption/desorption was recorded at 77 K on a Micromeritics TriStar II. Samples were degassed at 150 °C for 5 hours under vacuum prior to nitrogen physisorption measurements. Atomic resolution high-angle annular dark-field (HAADF) images were captured in a Nion UltraSTEM U100 operated at 60 keV and equipped with a Gatan Enfina electron energy loss spectrometer (EELS) at Oak Ridge National Laboratory. In addition, transmission electron microscopy (TEM), and high-resolution TEM (HRTEM) were performed on a probe-corrected FEI Titan 80-300 S/TEM at Brookhaven National Laboratory. Fe and Co K-edge X-ray absorption near edge structure (XANES) and extended X-ray absorption fine structure (EXAFS) experiments were carried out at beamline 12BM, Advanced Photon Source (APS), Argonne National Laboratory (ANL). Data reduction, data analysis, and EXAFS fitting were performed with the Athena, Artemis, and IFEFFIT software packages.

Electrochemical rotating-ring disk electrode (RRDE) test

Electrochemical measurements were conducted using an electrochemical workstation (CHI760b) coupled with an RRDE with a disk diameter of 5.6 mm in a three-electrode cell. A graphite rod and a Hg/HgSO₄ (K₂SO₄-sat.) electrode were used as the counter and reference electrodes, respectively. The reference electrode was calibrated to a reversible hydrogen electrode (RHE) in the same electrolyte before each measurement. To prepare the catalysts-modified electrode, the catalyst's ink was firstly prepared by adding 5 mg M-N-C catalysts in a vial containing 0.5 mL

Isopropyl alcohol and 15 μL Nafion® (5 wt.%) solution. Then the ink was drop-casted on the disk electrode with a designed loading of 0.6 mg cm^{-2} and dried at room temperature to yield a thin-film electrode. The catalyst-coated disk working electrode was subjected to cyclic voltammetry (CV) in O_2 -saturated $0.5 \text{ M H}_2\text{SO}_4$ at a scan rate of 100 mV s^{-1} to activate the catalysts. The electrocatalytic activity for ORR was tested by steady-state measurement using potential staircase control with a step of 0.05 V at intervals of 30 s from 1.0 to 0 V vs. RHE in O_2 -saturated $0.5 \text{ M H}_2\text{SO}_4$ solution at 25°C and a rotation rate of 900 rpm . Electron transfer number and H_2O_2 production were obtained by the following equations:

$$H_2O_2 \% = 200 \times \frac{I_r/N}{|I_d| + I_r/N} \quad (1)$$

$$n = 4 \times \frac{|I_d|}{|I_d| + I_r/N} \quad (2)$$

Whereas, I_r represents the ring current, I_d represents the disc current, N is the transfer efficiency.

Methanol tolerance ability tests were conducted by adding different concentrations of methanol into $0.5 \text{ M H}_2\text{SO}_4$ solution. The recovery tests were conducted after transferring the electrode back to the methanol-free $0.5 \text{ M H}_2\text{SO}_4$ solution. The stability tests were conducted by employing the potential cycling (0.6 to 1.0 V in O_2 sat. $0.5 \text{ M H}_2\text{SO}_4$, 50 mV s^{-1}) and by holding at the constant potential at 0.85 V during the ORR.

MEA preparation

Catalyst ink was prepared by ultrasonically mixing the catalyst, isopropanol, de-ionized water, and 5% Nafion® suspension (Ion Power). The catalysts-modified gas diffusion electrode (GDE) was prepared by manually blade printing of the catalysts ink onto the gas diffusion layer (GDL) until the cathode catalyst loading reached $\sim 4.0 \text{ mg cm}^{-2}$. The cathode and anode are hot-pressed (500 psi) onto a Nafion® 212 membrane at 130°C for 5 minutes. The geometric area of the membrane electrode assembly (MEA) was 5.0 cm^2 . Fuel cell testing was carried out in a single-cell fuel cell (Scribner) with single serpentine flow channels. The cells were all operated at 80°C .

For H₂-air/oxygen MEA, the commercial Pt/C-modified GDE (0.3 mg_{Pt} cm⁻², Fuel cell store) was used at the anode. Humidified hydrogen and air/oxygen were supplied to the anode and cathode at a flow rate of 200 sccm and 1000 sccm, respectively.

For methanol-air MEA, the commercial PtRu/C-modified GDE (Johnson Matthey) was used at the anode. Diluted methanol solutions were fed into the anode by a high-pressure liquid chromatography pump with flow rate of 0.5 mL min⁻¹. Humidified air was supplied to the cathode at a flow rate of 1000 sccm.

Active site quantification

The nitrite stripping method was employed for quantifying the density of active sites.¹ The 0.5 M acetate-buffer with pH=5.2 was prepared as the electrolyte. Typically, 1) the normal CV curves was firstly run in O₂-saturated electrolyte until the catalysts was stabilized and the ORR polarization curves was recorded before poison. 2) Record pre-baseline CVs in N₂-saturated electrolyte until the residual oxygen was removed, 1.0 V-0.3 V vs. RHE with scan rate of 5mV/s at rotating rate of 200 rpm. 3)Record a baseline CV in N₂-saturated electrolyte between 0.4V-(-0.2V), 10mV/s. 4) dip electrode into 125mM NaNO₂ solution for 5 mins at open circuit potential (OCP) at rotating speed of 300rpm. 4) rinse with water and dip electrode in DI water for 1 mins at OCP with 300 rpm, followed by in electrolyte for 5 mins at OCP and repeat with in DI water for another 1 min. 5) Record ORR polarization curve after poison in O₂-saturated electrolyte. 6) Record pre-baseline CVs in N₂-saturated electrolyte until the residual oxygen was removed, 1.0 V-0.3 V vs. RHE with scan rate of 5mV/s at rotating rate of 200 rpm. 7)Record stripping CV in N₂-saturated electrolyte between 0.4V-(-0.2V), 10mV/s. 8) Record recovery CV in N₂-saturated electrolyte between 0.4V-(-0.2V) after stripping, 10mV/s. 9) Record recovery ORR polarization curves in O₂-saturated electrolyte.

The following equation is used for quantifying the gravimetric site density (MSD) of catalysts:

$$MSD[mol\ sites\ g^{-1}] = \frac{Q_{strip}[Cg^{-1}]}{n_{strip}F[C\ mol^{-1}]}$$

Whereas, Q_{strip} is the integrated coulometric charge associated with the stripping peak, n_{strip} is the reduction of one adsorbed nitrosyl per site, *i.e.* 5. F is the Faraday constant.

Theoretical and Computational Section

All structure optimizations were carried out using the Perdew–Burke–Ernzerhof (PBE) functional of spin-polarized DFT as implemented in VASP 5.4.4¹⁻³ with the plane-wave basis sets of 400 eV cutoff kinetic energy to approximate the valence electron densities and the projector augmented wave (PAW) method to account for the core–valence interaction.⁴ The geometry optimization and self-consistent field convergence criterion were set to 0.01 eV/Å and 10⁻⁵ eV, respectively. The dispersion correction was considered by using the DFT-D3⁵ method to describe the van der Waals interactions. For the structure relaxation, we used 3×3×1 Monkhorst-Pack sampled k-points for the 6×6 graphene supercell with 15 Å of vacuum space to model the M-N-C materials. The Poisson–Boltzmann (PB) implicit solvation model, VaspSol,⁶ was used to describe the effect of solvation as implemented in VASP 5.4.4, with a dielectric constant $\epsilon=80$ for water.

In the charge-neutral method (cnm), the adsorption energy of methanol molecule (ΔE_{ads}) is calculated as

$$\Delta E_{\text{ads}} = E(\text{CH}_3\text{OH}^*) - E(^*) - E(\text{CH}_3\text{OH}(\text{sol})) \quad (1)$$

where $E(\text{CH}_3\text{OH}^*)$ and $E(^*)$ are the total energies of the catalyst with and without CH₃OH molecule adsorption; $E(\text{CH}_3\text{OH}(\text{sol}))$ is the energy of the CH₃OH molecule in solution.

To consider the charge effects, constant-potential (μ_e) method⁷⁻⁹ was adopted based on the VaspSol implicit solvation model. Along with the geometry relaxation, the number of electrons is optimized in each step to match the applied potential. As the geometry relaxation converges, we make sure the charge and the Fermi level of the system are also converged. The ΔE_{ads} becomes

$$\Delta E_{\text{ads}} = E(\text{CH}_3\text{OH}^*) - E(^*) - E(\text{CH}_3\text{OH}) + (Q2 - Q1)\mu_e \quad (2)$$

where $Q1$ and $Q2$ are the net charges on the catalyst before and after CH₃OH adsorption, which are determined by the constraint

$$E_{\text{F}}(^*Q1) = E_{\text{F}}(\text{CH}_3\text{OH}^*Q2) = \mu_e \quad (3)$$

Where μ_e refers to the electron energy in reversible hydrogen electrode (RHE) (i.e. $U_{\text{RHE}} = \mu_e - \mu_{\text{SHE}} + 0.059 \cdot \text{pH}$) and thus are U_{RHE} dependent. The subscript “cpm” emphasizes that the μ_e (and

consequently the E_F is fixed during the reaction; thus, this method is called constant-potential method (cpm).

Supporting Figures

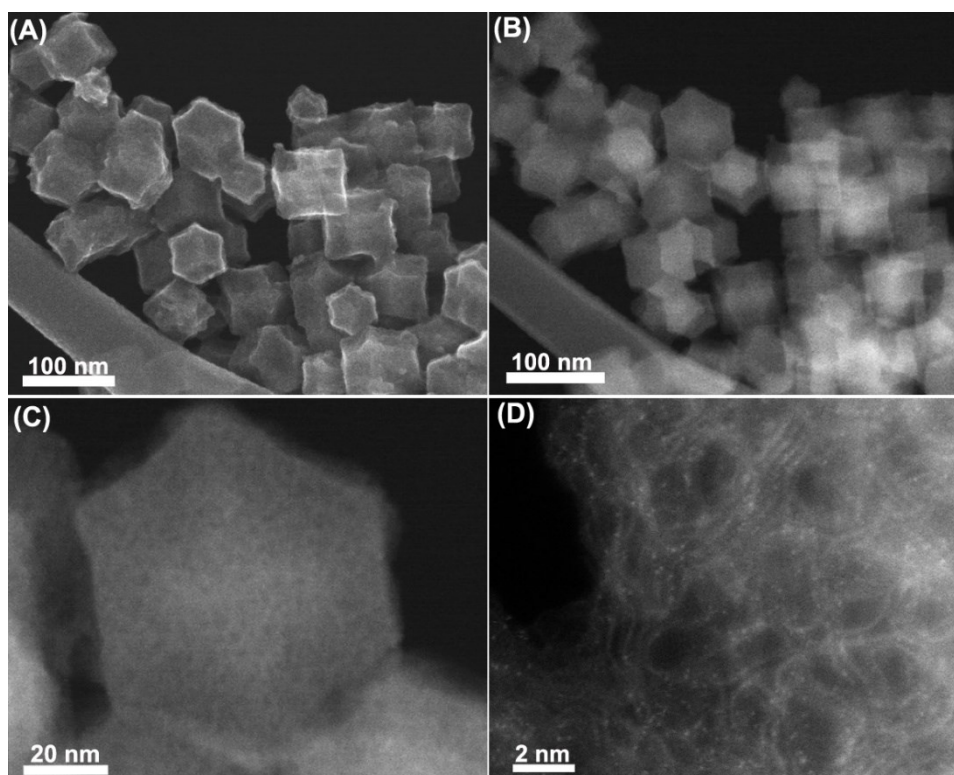


Fig. S1. (A) HAADF-SEM, (B) HAADF-STEM images, and (C and D) high-resolution HAADF-STEM images of Fe-N-C catalyst (~65 nm).

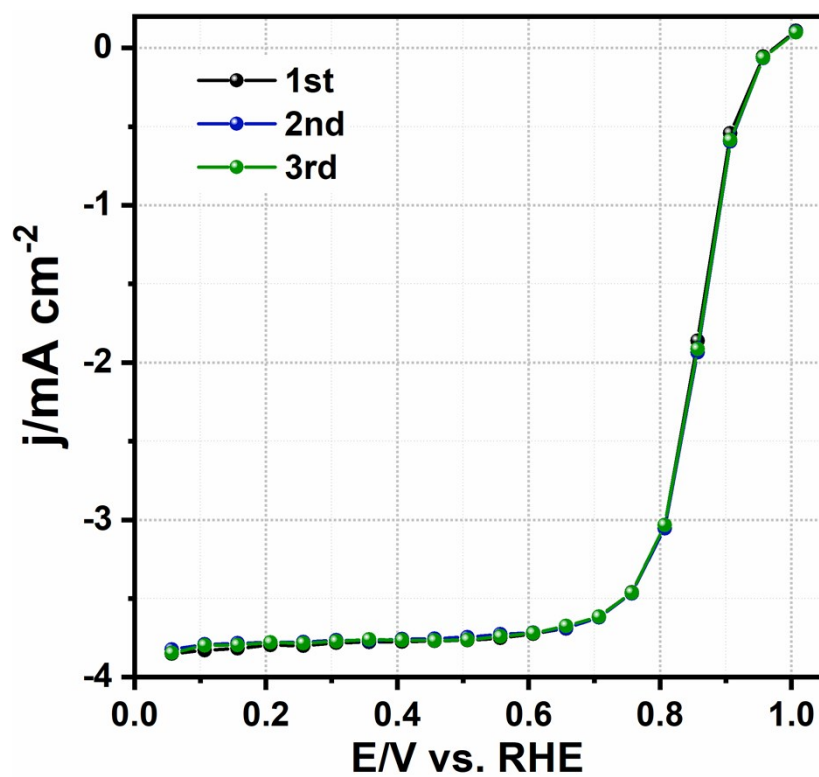


Fig. S2. ORR polarization plots of the Fe-N-C catalysts in O₂ saturated 0.5 M H₂SO₄ with a rotating rate of 900 rpm. Each polarization plot was obtained after 40 segments cyclic voltammetry (CV) test with a potential window of 0-1.0 V vs. RHE.

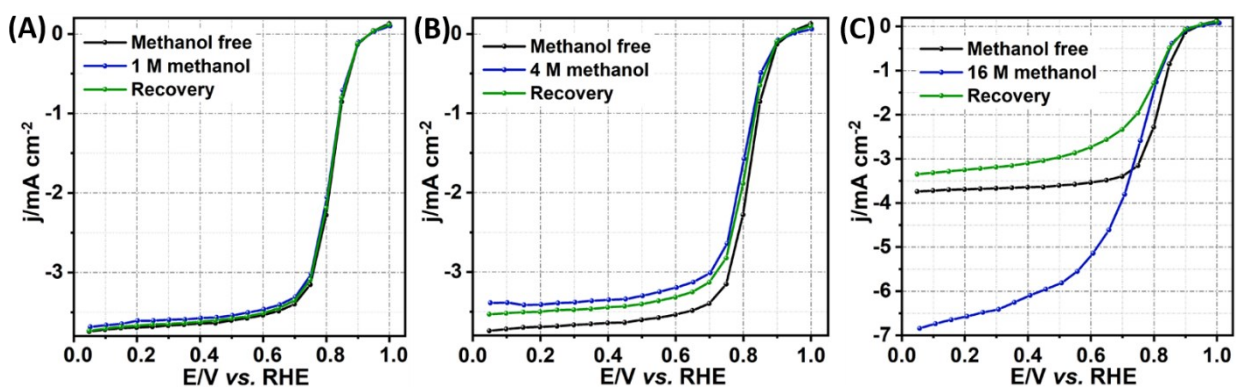


Fig. S3. ORR polarization plots of the Fe-N-C catalysts achieved in O_2 -saturated 0.5 M H_2SO_4 containing 1 M (A), 4M (B) and 16 M methanol (C) (blue lines), and their rinse recovery polarization plots (green lines) obtained by transfer the electrode back to methanol-free electrolyte with a rotating rate of 900 rpm.

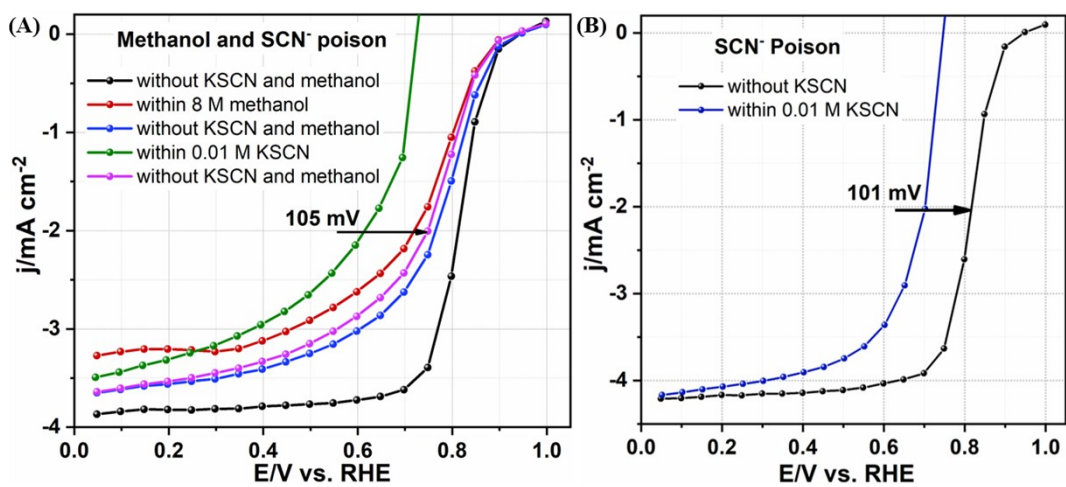


Fig. S4. ORR polarization plots of the Fe-N-C catalysts achieved in O₂-saturated 0.5 M H₂SO₄ aqueous solution with and without methanol and KSCN (A) and in methanol-free O₂-saturated 0.5 M H₂SO₄ electrolyte containing KSCN (B) with a rotating rate of 900 rpm.

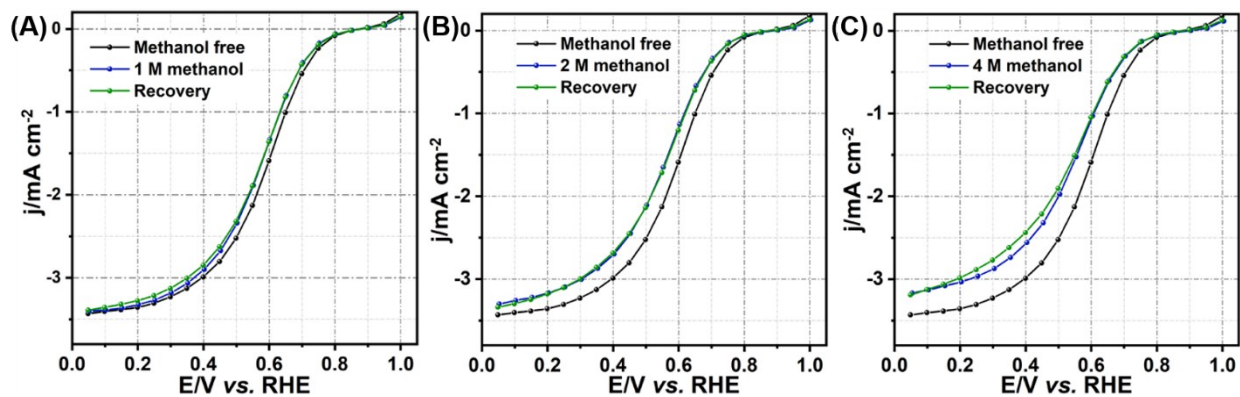


Fig. S5. ORR polarization plots of N-C catalysts achieved in O_2 -saturated 0.5 M H_2SO_4 containing 1 M (A), 2M (B) and 4 M methanol (C) (blue lines), and their rinse recovery polarization plots (green lines) obtained by transferring the electrode back to methanol-free electrolyte with a rotating rate of 900 rpm.

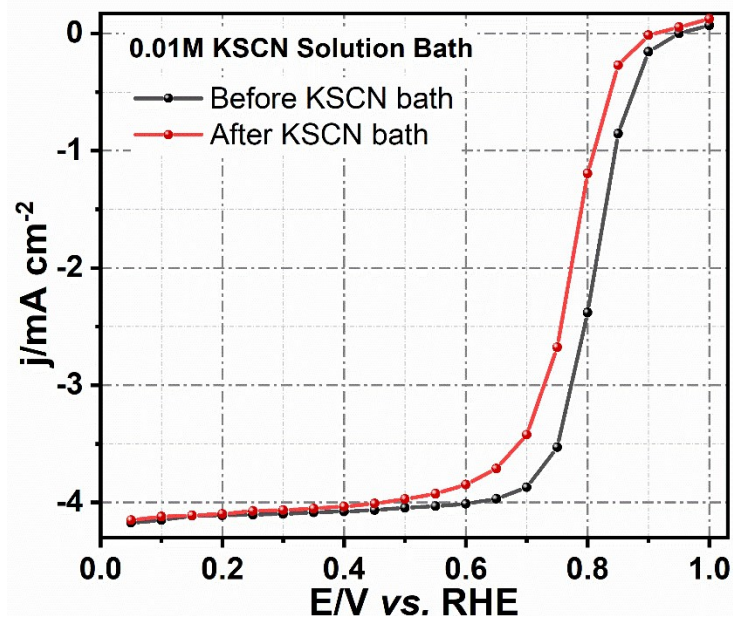


Fig. S6. ORR polarization plots of the Fe-N-C catalysts in O₂-saturated 0.5 M H₂SO₄ aqueous solution before and after 0.01 M KSCN solution bath with a rotating rate of 900 rpm.

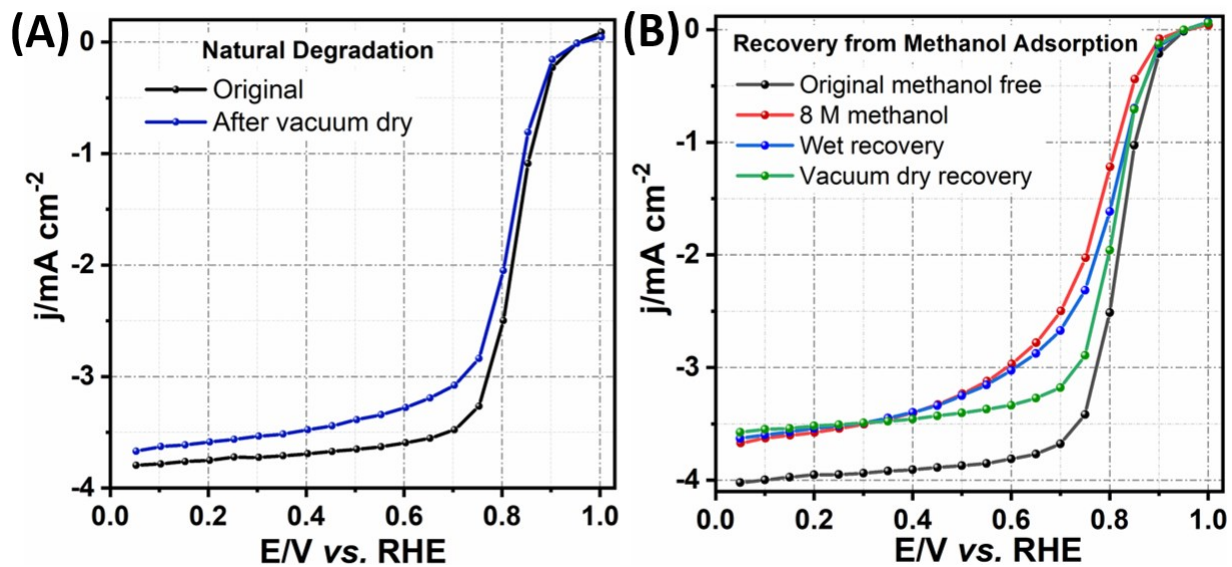


Fig. S7. ORR polarization plots of the Fe-N-C catalysts in O_2 -saturated 0.5 M H_2SO_4 aqueous solution before and after vacuum drying: (A) without methanol adsorption (natural degradation after drying just used for comparison); (B) with methanol adsorption.

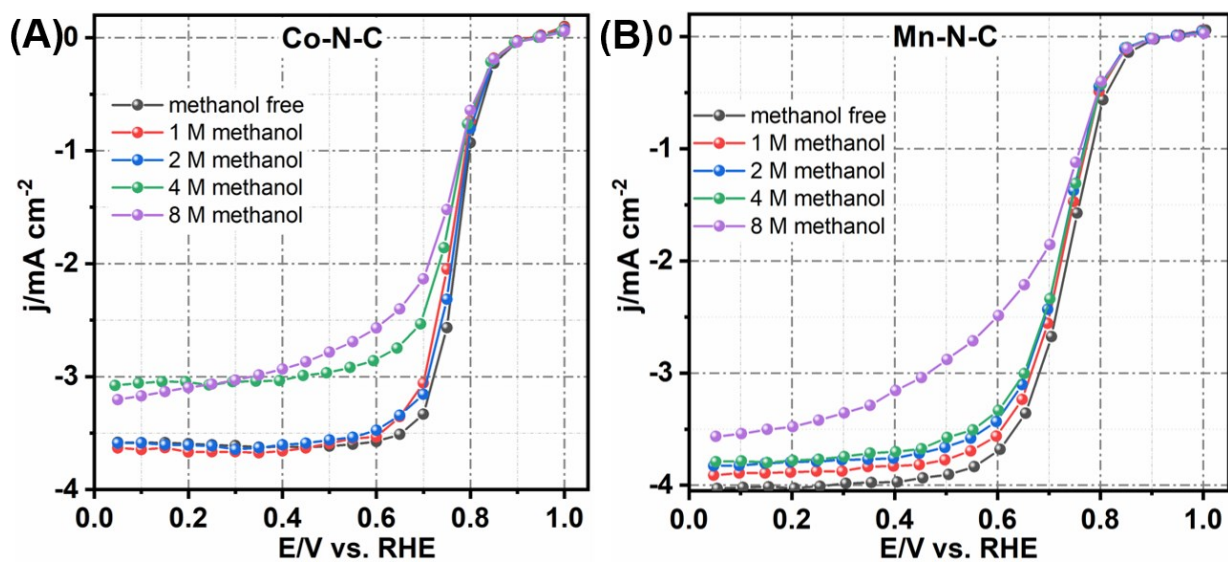


Fig. S8. ORR polarization plots of the (A) Co-doped ZIF-8-derived Co-N-C and (B) Mn-doped ZIF-8-derived Mn-N-C catalysts in O₂-saturated 0.5 M H₂SO₄ aqueous solution containing different methanol concentrations with a rotating rate of 900 rpm, respectively.

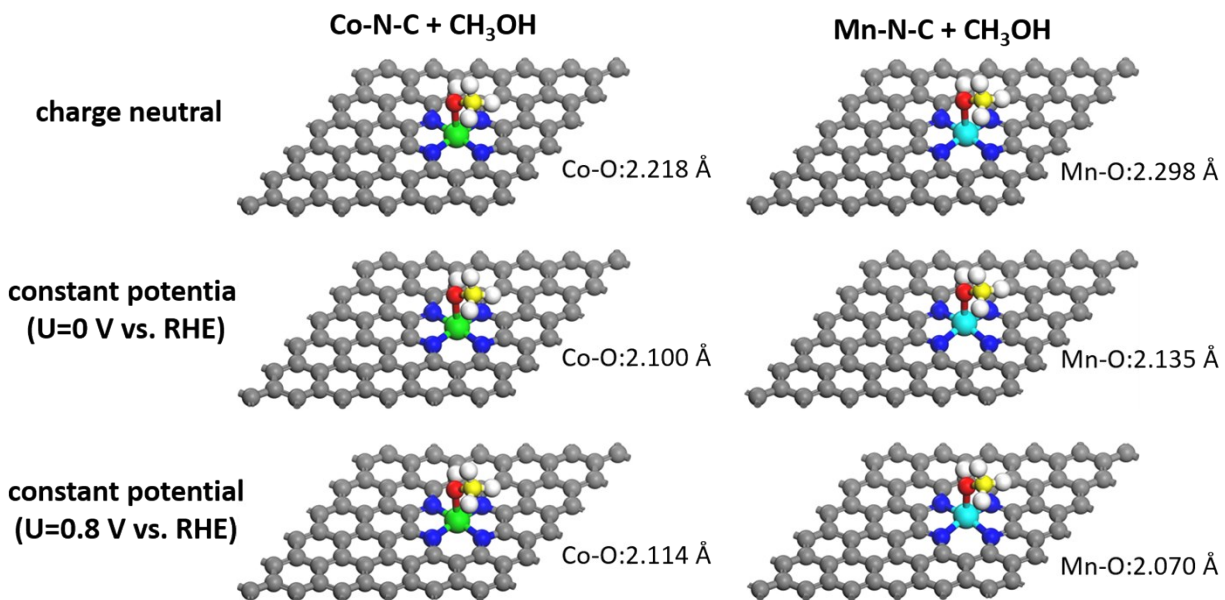


Fig. S9. Adsorption mode of CH₃OH on the Co-N-C and Mn-N-C catalysts as obtained using DFT with PBE functional through the charge-neutral and at constant potential method ($U=0$ and 0.8 V).

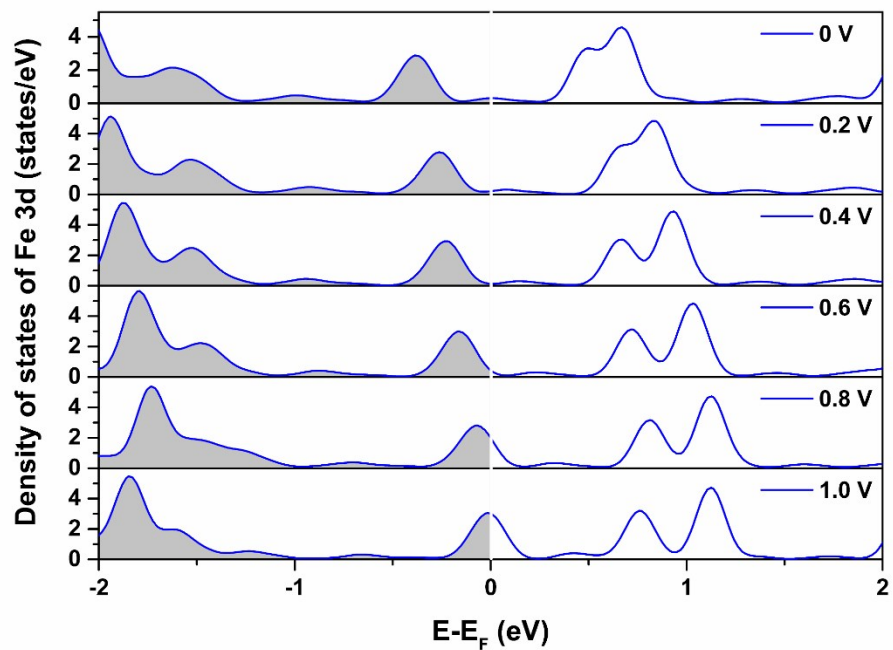


Fig. S10. Electronic Density of States (DOS) of Fe 3d for charged Fe-N-C catalyst at $U = 0 - 1.0$ V vs. RHE. The Fermi level is set as zero.

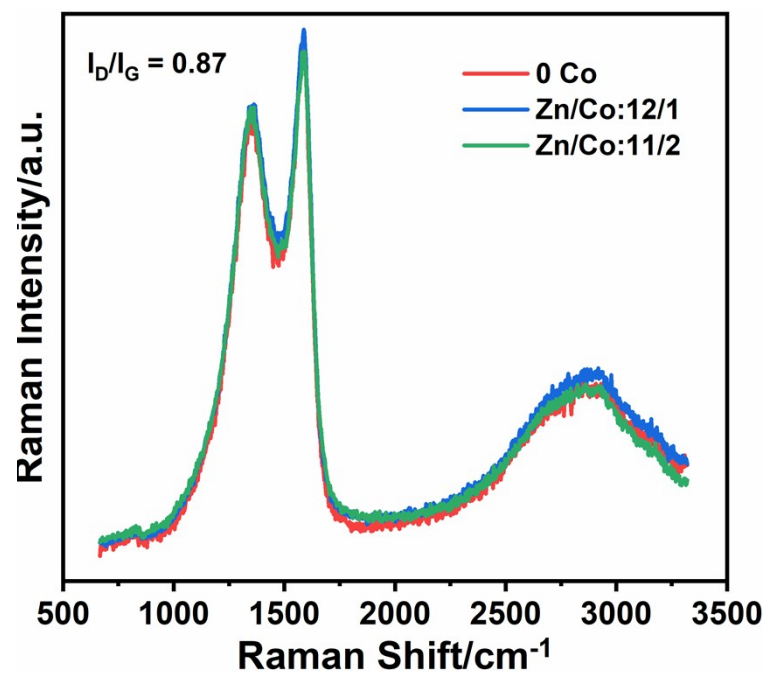


Fig. S11. Raman spectrum of the N-C and Co-N-C electrocatalysts, respectively.

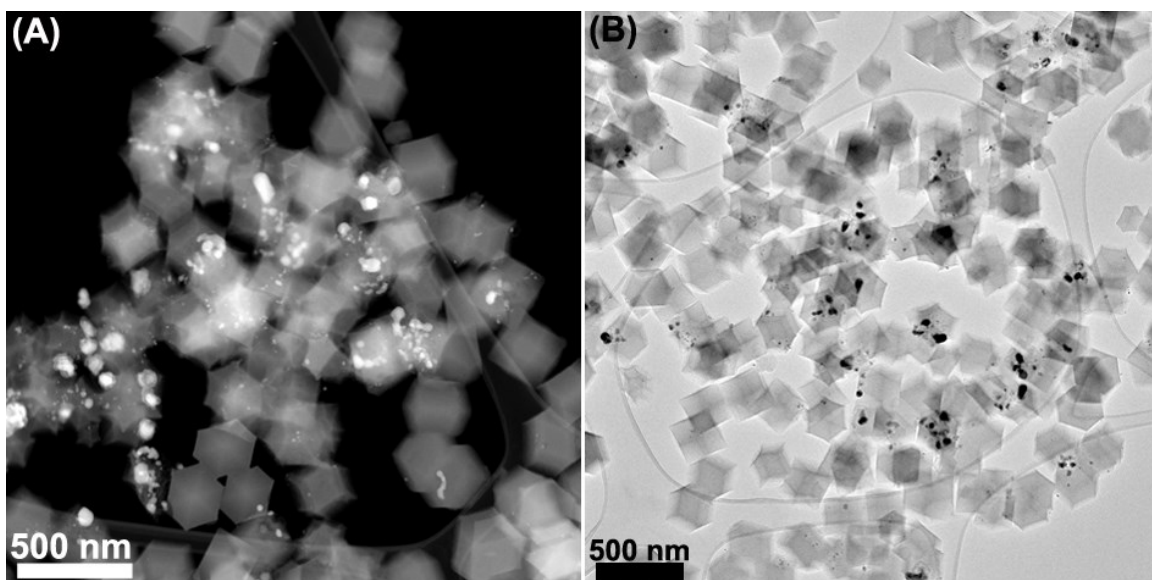


Fig. S12. (A) HAADF-STEM image and (B) TEM image of the Co-N-C catalysts derived from Co-doped ZIF-8 nanocrystals synthesized with the Zn/Co precursor feeding ratio above 9/4.

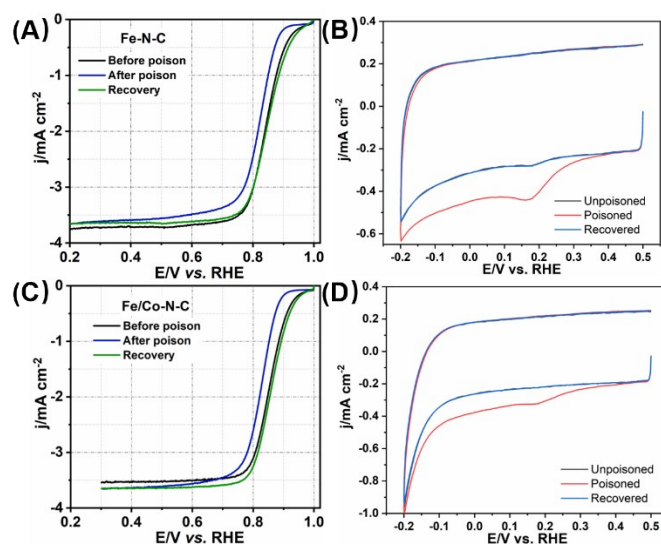


Fig. S13. (A and C) ORR polarization curves of Fe-N-C and Fe/Co-N-C catalysts before and after nitrite poison in O_2 -saturated 0.5 M acetate buffer with $\text{pH}=5.2$, recorded at 900 rpm with scan rate of 5 mV/s, respectively. (B and D) CV curves of the catalysts before and after nitrite stripping recorded in N_2 -saturated 0.5 M acetate buffer with $\text{pH}=5.2$ and scan rate of 10mV/s.

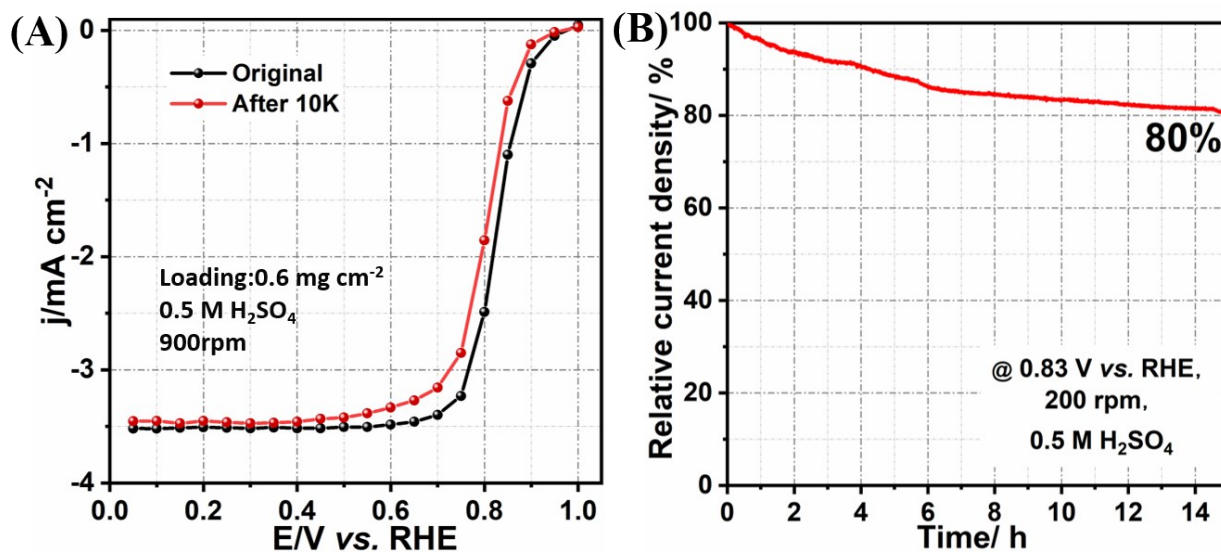


Fig. S14. (A) ORR polarization curves of Fe/Co-N-C catalysts before and after potential static test between 0-1.0 V for 10 K cycles, (B) Amperometric i - t curve of Fe/Co-N-C catalysts tested at 0.83 V vs. RHE in O_2 -saturated 0.5 M H_2SO_4 electrolyte.

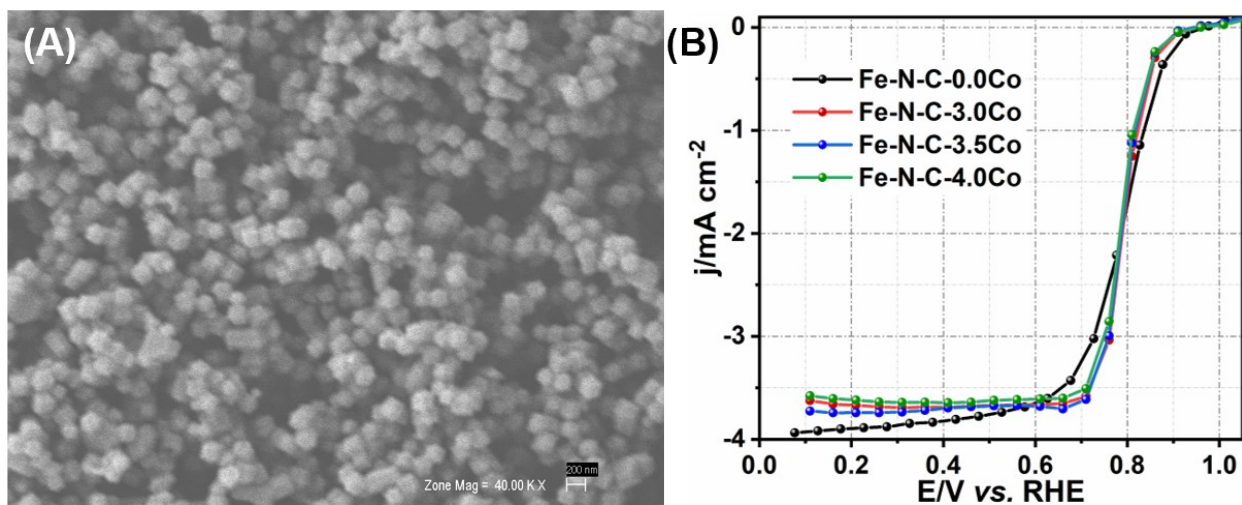


Fig. S15. (A) SEM image of as obtained Co/Fe-N-C (Fe-N-C-3.5 Co) and (B) ORR activity of Co/Fe-N-C catalysts obtained by firstly pre-doping Fe and second Co adsorption. The Co adsorption molar ratio is controlled the same with Fe adsorption molar in the Fe/Co-N-C catalysts.

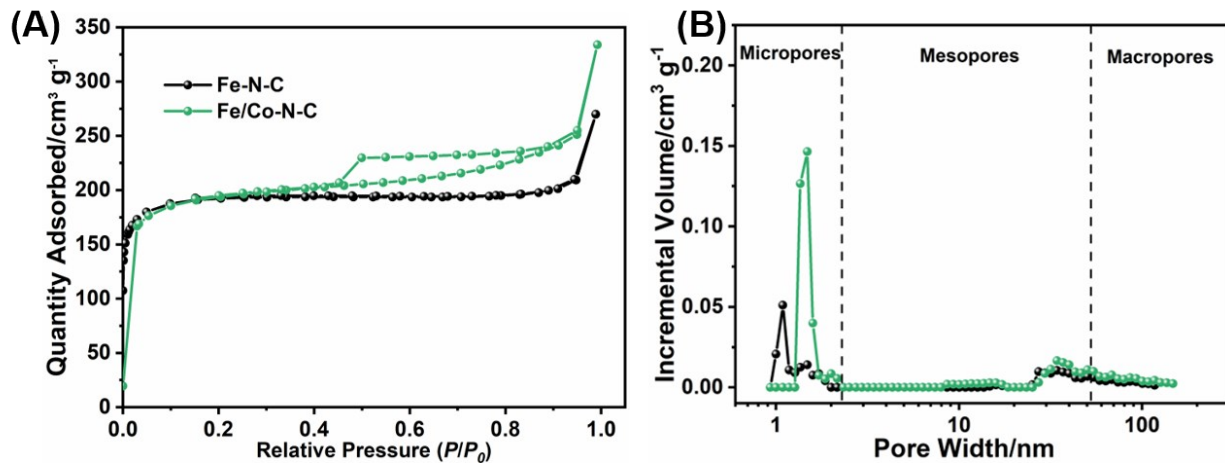


Fig. S16. (A) Nitrogen adsorption-desorption isotherm curves and (B) pore distribution of the as-derived Fe/Co-N-C (11/2) and Fe-N-C electrocatalysts, respectively.

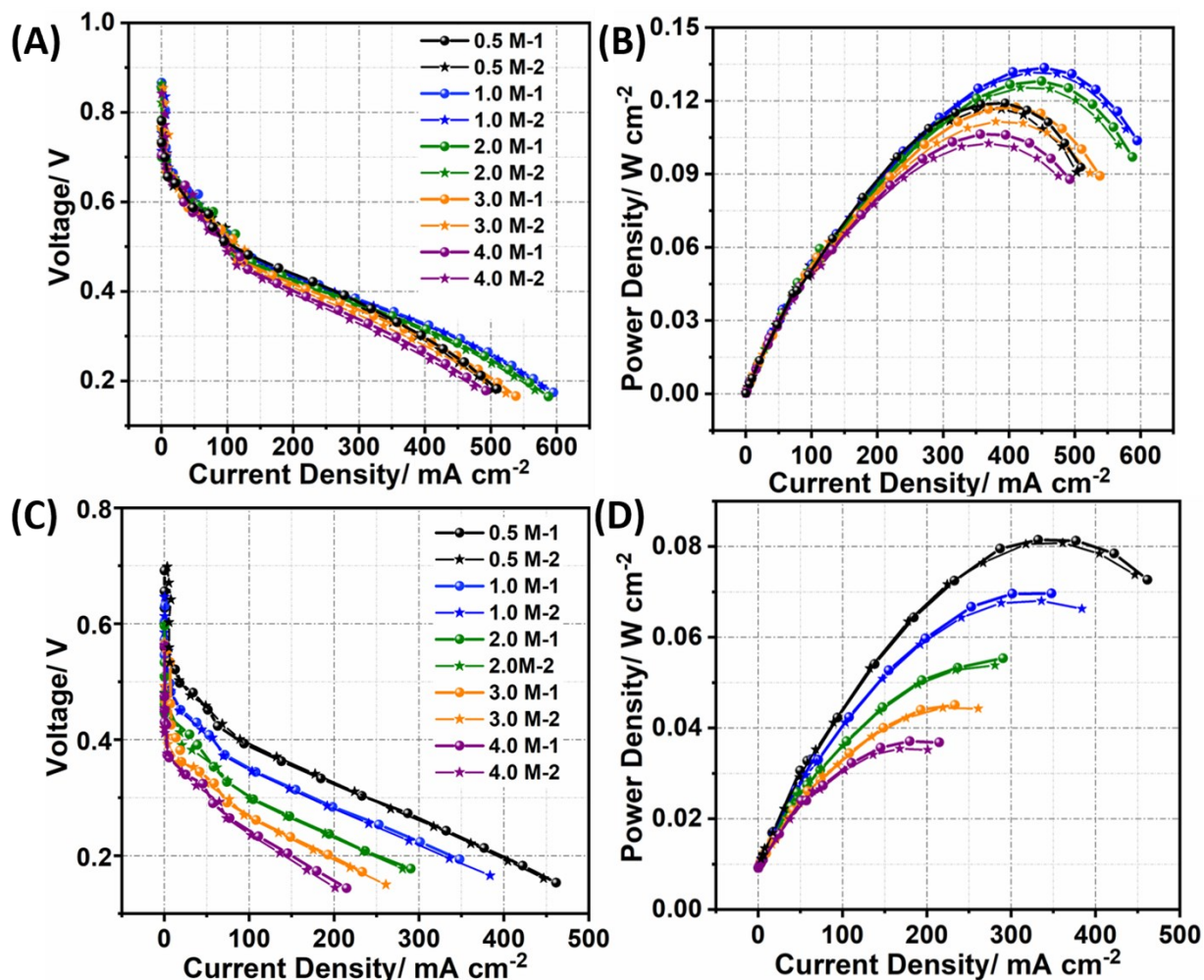


Fig S17. Polarization plots of (A and C) cell voltage and (B and D) power density versus current density of methanol-air cell using Fe/Co-N-C (11/2) (A and B) and commercial Pt/C (C and D) as cathode catalysts as a function of methanol concentration. Each methanol concentration was continuously tested twice. Anode: 4.0 mg cm^{-2} PtRu/C; cathode: 5.0 mg cm^{-2} Fe/Co-N-C(11/2) or 0.9 mg cm^{-2} Pt/C; 0.5 mL min^{-1} methanol flow rate; 1.0 atm air 1000 mLmin^{-1} flow rate; membrane: Nafion 212; cell: $80 \text{ }^\circ\text{C}$.

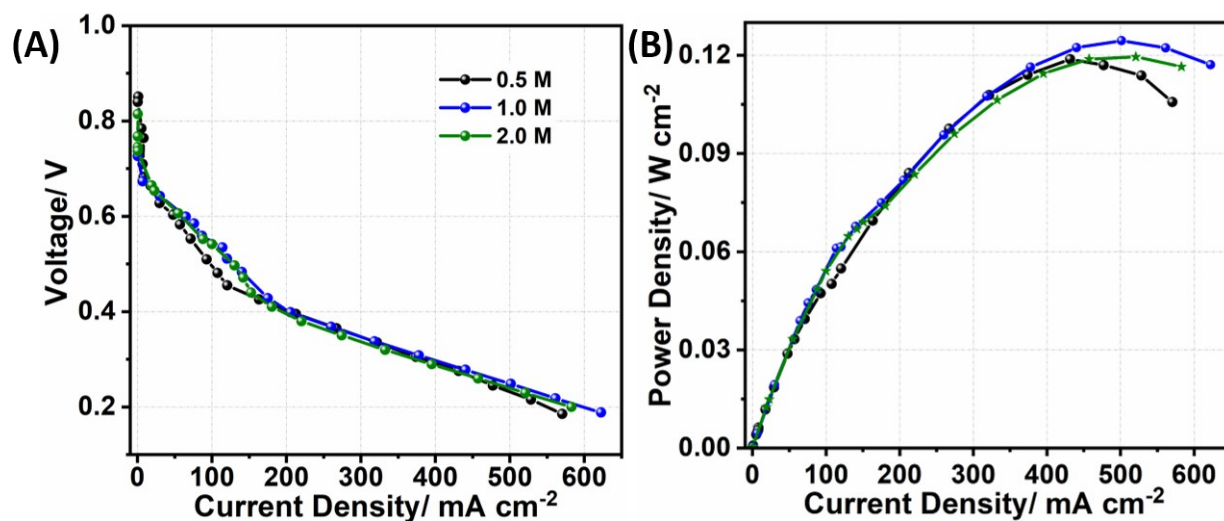


Fig. S18. Polarization plots of cell voltage and power density versus current density of methanol-air cell using Fe-N-C (13:0) as cathode catalysts as a function of methanol concentration. Each methanol concentration was continuously tested twice. Anode: 3.5 mg cm⁻² PtRu/C; cathode: 3.6 mg cm⁻² Fe-N-C; 0.5 mL min⁻¹ 3.0 M methanol flow rate; 1.0 atm air 1000 mLmin⁻¹ flow rate; membrane: Nafion 212; cell: 80 °C. Fe-N-C catalysts were synthesized via the same method except for the Co-doping in the first step and with 3.5 mg FeCl₃ in the solution in the second adsorption step.

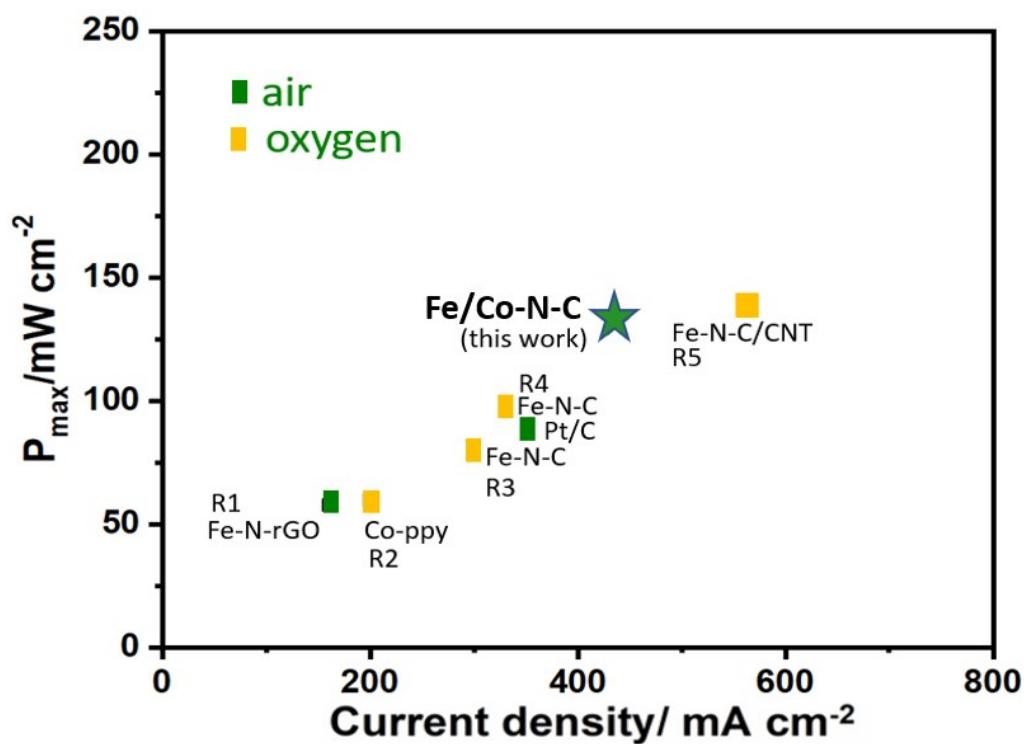


Fig. S19. Comparison of the MEA peak power density of the methanol-air/oxygen cell of other previous reported catalysts. ¹⁰⁻¹⁴

Supporting Tables

Table S1. XRF analysis of secondary heat treatment and Co-doping effect on the Co and Zn content in the catalysts.

| Sample | C | Zn | Co |
|------------------------------------|---------|---------|--------|
| ZIF-8-1100C 1h | 99.92 % | 826 ppm | - |
| ZIF-8-900C 1h + 1100C 1h | 99.93 % | 478 ppm | - |
| (12/1) Co-ZIF-8-900C 1h + 1100C 1h | 99.99 % | 51 ppm | 52 ppm |

Table S2. Comparison of the MEA performance of H₂-air/O₂ fuel cell using M-N-C catalysts.

| Catalysts | Half-wave potential | Electrolyte | Fuel cell performance | Ref. |
|---------------------------------|---------------------|--------------------------------------|--|------|
| Co/Zn(mIm) ₂ -P | 0.76 V | 0.1 M HClO ₄ | 0.374 W cm ⁻² | 15 |
| 20Co-NC-1100 | 0.8 V | 0.5 M H ₂ SO ₄ | H ₂ /O ₂ : 0.56 W cm ⁻² ; H ₂ /air: 0.28 W cm ⁻² | 16 |
| Co-N-C@F127 | 0.84 V | 0.5 M H ₂ SO ₄ | H ₂ /O ₂ : 0.87 W cm ⁻² ; H ₂ /air: 0.28 W cm ⁻² | 17 |
| FeNC-1000 | 0.804 V | 0.5 M H ₂ SO ₄ | H ₂ /O ₂ : 1.01 W cm ⁻² | 18 |
| (CM+PANI)-Fe-C | 0.80 V | 0.5 M H ₂ SO ₄ | H ₂ /O ₂ : 0.87 W cm ⁻² ; H ₂ /air: 0.42 W cm ⁻² | 19 |
| PANI-Fe-MCS | 0.80 V | 0.5 M H ₂ SO ₄ | H ₂ /O ₂ : 0.83 W cm ⁻² ; | 20 |
| Fe-NC-Phen-PANI | 0.80 V | 0.5 M H ₂ SO ₄ | H ₂ /O ₂ : 0.86 W cm ⁻² ; H ₂ /air: 0.38 W cm ⁻² | 21 |
| TPI@Z8(SiO ₂)-650-C | / | / | H ₂ /2.5 bar O ₂ : 1.18 W cm ⁻² ; H ₂ /air: 0.42 W cm ⁻² | 22 |
| Fe,Co/N-C | 0.84V | 0.1 M HClO ₄ | H ₂ /air: 0.50 W cm ⁻² | 23 |

Table S3. Fitting parameters of the Co K-edge EXAFS for CoPc standard and Fe/Co-N-C (CN: coordination number, R: bond distance; σ^2 : mean-square disorder; E₀: energy shift). The single-

digit numbers in parentheses are the last digit errors. The numbers in parentheses for CN are the full errors.

| | Scattering Path | CN | R (Å) | E_0 (eV) | σ^2 (Å ²) |
|-----------|-----------------|-----------|---------|------------|------------------------------|
| CoPc | Co-N | 4 | 1.92(1) | | 0.0024(7) |
| | Co-C | 8 | 2.95(1) | | 0.0032(4) |
| | Co-N-C | 16 | 3.11(1) | | 0.0205(1) |
| | Co-N | 4 | 3.35(1) | 6(1) | 0.0090(5) |
| | Co-N | 4 | 3.84(1) | | 0.0008(1) |
| | Co-C | 6 | 4.17(1) | | 0.0200(5) |
| | Co-N-C | 12 | 4.20(1) | | 0.0038(8) |
| | Co-N-C-N | 6 | 4.22(1) | | 0.0008(5) |
| Fe/Co-N-C | Co-N | 4.6(1.2) | 1.92(2) | | 0.0142(4) |
| | Co-C | 9.2(2.3) | 2.97(3) | -10(2) | 0.0117(2) |
| | Co-N-C | 18.5(4.6) | 3.13(3) | | 0.0029(4) |

Table S4. Fitting parameters of the Fe K-edge EXAFS for FePc standard and Fe/Co-N-C (CN: coordination number, R: bond distance; σ^2 : mean-square disorder; E_0 : energy shift). The single-

digit numbers in parentheses are the last digit errors. The numbers in parentheses for CN are the full errors.

| | Scattering Path | CN | R (Å) | E_0 (eV) | $\sigma^2(\text{Å}^2)$ |
|-----------|-----------------|-----------|---------|------------|------------------------|
| FePc | Fe-N | 4 | 1.93(1) | | 0.0078(9) |
| | Fe-C | 8 | 2.96(1) | | 0.0078(1) |
| | Fe-N-C | 16 | 3.13(2) | | 0.0040(6) |
| | Fe-N | 4 | 3.37(2) | | 0.0065(8) |
| | Fe-N-N | 16 | 3.86(2) | -5(2) | 0.0008(7) |
| | Fe-N-N | 4 | 3.86(2) | | 0.0008(7) |
| | Fe-C | 6 | 4.19(2) | | 0.0184(6) |
| | Fe-N-C | 12 | 4.22(2) | | 0.0107(2) |
| Fe/Co-N-C | Fe-N | 3.9(0.7) | 2.01(2) | | 0.0101(1) |
| | Fe-C | 7.7(1.3) | 3.04(3) | 3(2) | 0.0110(5) |
| | Fe-N-C | 15.5(2.6) | 3.26(2) | | 0.0026(7) |

References

1. G. Kresse and J. Furthmuller, *Phys. Rev. B*, 1996, **6**, 15-50.

2. G. Kresse and J. Furthmuller, *Phys. Rev. B*, 1996, **54**, 11169-11186.
3. J. P. Perdew, K. Burke and M. Ernzerhof, *Phys. Rev. Lett.*, 1996, **77**, 3865-3868.
4. G. Kresse and D. Joubert, *Phys. Rev. B*, 1999, **59**, 1758-1775.
5. S. Grimme, J. Antony, S. Ehrlich and H. Krieg, *J. Chem. Phys.*, 2010, **132**, 154104.
6. K. Mathew, R. Sundararaman, K. Letchworth-Weaver, T. A. Arias and R. G. Hennig, *J. Chem. Phys.*, 2014, **140**, 084106.
7. D. Kim, J. Shi and Y. Liu, *J. Am. Chem. Soc.*, 2018, **140**, 9127-9131.
8. X. Zhao and Y. Liu, *J. Am. Chem. Soc.*, 2020, **142**, 5773-5777.
9. X. Zhao, J. Shi, Y. Ji and Y. Liu, *WIREs Comput. Mol. Sci.*, 2019, **9**, e1418.
10. Q. Li, T. Y. Wang, D. Havas, H. G. Zhang, P. Xu, J. T. Han, J. Cho and G. Wu, *Adv. Sci.*, 2016, **3**.
11. A. L. M. Reddy, N. Rajalakshmi and S. Ramaprabhu, *Carbon*, 2008, **46**, 2-11.
12. X. Xu, Z. Xia, X. Zhang, R. Sun, X. Sun, H. Li, C. Wu, J. Wang, S. Wang and G. Sun, *Appl. Catal. B: Environ.*, 2019, **259**, 118042.
13. Y.-C. Wang, L. Huang, P. Zhang, Y.-T. Qiu, T. Sheng, Z.-Y. Zhou, G. Wang, J.-G. Liu, M. Rauf and Z.-Q. Gu, *ACS Energy Lett.*, 2017, **2**, 645-650.
14. Z. Xia, X. Xu, X. Zhang, H. Li, S. Wang and G. Sun, *J. Mater. Chem. A*, 2020.
15. L. Chong, G. A. Goenaga, K. Williams, H. M. Barkholtz, L. R. Grabstanowicz, J. A. Brooksbank, A. B. Papandrew, R. Elzein, R. Schlaf and T. A. Zawodzinski Jr, *ChemElectroChem*, 2016, **3**, 1541-1545.
16. X. X. Wang, D. A. Cullen, Y. T. Pan, S. Hwang, M. Wang, Z. Feng, J. Wang, M. H. Engelhard, H. Zhang and Y. He, *Adv. Mater.*, 2018, **30**, 1706758.
17. Y. He, S. Hwang, D. A. Cullen, M. A. Uddin, L. Langhorst, B. Li, S. Karakalos, A. J. Kropf, E. C. Wegener, J. Sokolowski, M. Chen, D. Myers, D. Su, K. L. More, G. Wang, S. Litster and G. Wu, *Energy Environ. Sci.*, 2019, **12**, 250-260.
18. Y. Li, X. Liu, L. Zheng, J. Shang, X. Wan, R. Hu, X. Guo, S. Hong and J. Shui, *J. Mater. Chem. A*, 2019, **7**, 26147-26153.
19. H. T. Chung, D. A. Cullen, D. Higgins, B. T. Sneed, E. F. Holby, K. L. More and P. Zelenay, *Science*, 2017, **357**, 479-484.
20. X. Fu, F. M. Hassan, P. Zamani, G. Jiang, D. C. Higgins, J.-Y. Choi, X. Wang, P. Xu, Y. Liu and Z. Chen, *Nano Energy*, 2017, **42**, 249-256.

21. X. Fu, P. Zamani, J. Y. Choi, F. M. Hassan, G. Jiang, D. C. Higgins, Y. Zhang, M. A. Hoque and Z. Chen, *Adv. Mater.*, 2017, **29**, 1604456.
22. X. Wan, X. Liu, Y. Li, R. Yu, L. Zheng, W. Yan, H. Wang, M. Xu and J. Shui, *Nat. Catal.*, 2019, **2**, 259-268.
23. J. Wang, Z. Huang, W. Liu, C. Chang, H. Tang, Z. Li, W. Chen, C. Jia, T. Yao and S. Wei, *J. Am. Chem. Soc.*, 2017, **139**, 17281-17284.